



# **JGR Space Physics**

## RESEARCH ARTICLE

10.1029/2022JA030932

#### **Key Points:**

- We report quasi-periodic energetic electron precipitation observed by low-altitude Electron Losses and Fields Investigation CubeSats
- Quasi-periodicity of the precipitation is due to periodicity of whistler-mode wave generation at the equator
- Whistler-mode wave generation is modulated by ultra-low-frequency waves seen within a large magnetic local time, L-shell domain

#### **Supporting Information:**

Supporting Information may be found in the online version of this article.

#### Correspondence to:

X. Shi, sxf1698@g.ucla.edu

#### Citation:

Shi, X., Zhang, X.-J., Artemyev, A., Angelopoulos, V., Hartinger, M. D., Tsai, E., & Wilkins, C. (2022). On the role of ULF waves in the spatial and temporal periodicity of energetic electron precipitation. *Journal of Geophysical Research: Space Physics*, 127, e2022IA030932. https://doi.org/10.1029/2022JA030932

Received 15 AUG 2022 Accepted 2 DEC 2022

# On the Role of ULF Waves in the Spatial and Temporal Periodicity of Energetic Electron Precipitation

Xiaofei Shi<sup>1</sup>, Xiao-Jia Zhang<sup>1</sup>, Anton Artemyev<sup>1</sup>, Vassilis Angelopoulos<sup>1</sup>, Michael D. Hartinger<sup>1,2</sup>, Ethan Tsai<sup>1</sup>, and Colin Wilkins<sup>1</sup>

<sup>1</sup>Department of Earth, Planetary, and Space Sciences, University of California, Los Angeles, CA, USA, <sup>2</sup>Space Science Institute, Boulder, CO, USA

**Abstract** Energetic electron precipitation to the Earth's atmosphere is a key process controlling radiation belt dynamics and magnetosphere-ionosphere coupling. One of the main drivers of precipitation is electron resonant scattering by whistler-mode waves. Low-altitude observations of such precipitation often reveal quasi-periodicity in the ultra-low-frequency (ULF) range associated with whistler-mode waves, causally linked to ULF-modulated equatorial electron flux and its anisotropy. Conjunctions between ground-based instruments and equatorial spacecraft show that low-altitude precipitation concurrent with equatorial whistler-mode waves also exhibits a spatial periodicity as a function of latitude over a large spatial region. Whether this spatial periodicity might also be due to magnetospheric ULF waves spatially modulating electron fluxes and whistler-mode chorus has not been previously addressed due to a lack of conjunctions between equatorial spacecraft, low earth orbit spacecraft, and ground-based instruments. To examine this question, we combine ground-based and equatorial observations magnetically conjugate to observations of precipitation at the low-altitude, polar-orbiting CubeSats Electron Losses and Fields Investigation-A and -B. As they sequentially cross the outer radiation belt with a temporal separation of minutes to tens of minutes, they can easily reveal the spatial quasi-periodicity of electron precipitation. Our combined data sets confirm that ULF waves may modulate whistler-mode wave generation within a large magnetic local time and L-shell domain in the equatorial magnetosphere, and thus lead to significant aggregate energetic electron precipitation exhibiting both temporal and spatial periodicity. Our results suggest that the coupling between ULF and whistler-mode waves is important for outer radiation belt dynamics.

# 1. Introduction

Resonant scattering of energetic electrons from Earth's radiation belts by electromagnetic whistler-mode waves is the main driver of energetic electron precipitation from the outer radiation belt to the atmosphere (e.g., W. Li & Hudson, 2019; Millan & Thorne, 2007; Thorne et al., 2021). Statistical analyses of observed wave characteristics (e.g., O. V. Agapitov et al., 2013; W. Li, Thorne, Bortnik, Shprits, et al., 2011; Meredith et al., 2012), coupled with global numerical simulations of resonant scattering, can provide estimates of long-term electron losses due to precipitation (e.g., Hsieh et al., 2022; Mourenas et al., 2014; Ma et al., 2018, 2020; Orlova et al., 2016, and references therein). Conversely, case studies using equatorial spacecraft observations of wave and plasma characteristics specific for each event can describe well the dynamics of resonant electron fluxes, which are often localized (e.g., O. V. Agapitov et al., 2015; Capannolo et al., 2019; Foster et al., 2014; Gan et al., 2020). Neither statistical nor equatorial spacecraft case studies can separate the temporal and spatial (mesoscale,  $\sim R_E$  at the equator) variations of precipitation. However, multi-spacecraft measurements at low altitudes or correlative studies using low-altitude and equatorial measurements can be used to infer such scales. These two approaches were employed to study the most intense but highly transient and localized precipitation events, microbursts (Douma et al., 2017; O'Brien et al., 2004), by Shumko et al. (2018) and (e.g., Breneman et al., 2015; Mozer et al., 2018; Shumko et al., 2021), respectively. Mesoscale precipitation events, with temporal and spatial scales comparable to those of equatorial chorus waves (O. V. Agapitov et al., 2017; O. Agapitov, Mourenas, Artemyev, Mozer, Hospodarsky et al., 2018), have yet to be investigated with similar methods.

A classical example of dynamic precipitation is the pulsating aurora (Belon et al., 1969; Coroniti & Kennel, 1970; Johnstone, 1978; McEwen et al., 1981), which is associated with ~10 keV electron precipitation as a result of quasi-periodic whistler-mode (chorus) wave scattering (Kasahara et al., 2018; Nishimura et al., 2010). The quasi-periodicity of these wave emissions may be caused by usltra-low-frequency (ULF) waves modulating

© 2022. American Geophysical Union. All Rights Reserved.

SHI ET AL. 1 of 12

plasma and energetic electron fluxes around the equator (Bryant et al., 1971; Coroniti & Kennel, 1970; Jaynes, Lessard, et al., 2015; W. Li, Bortnik, et al., 2011; W. Li, Thorne, Bortnik, Nishimura, & Angelopoulos, 2011; L. Li et al., 2022; Motoba et al., 2013; Watt et al., 2011). Recent optical and low-altitude measurements showed that ≤10 keV precipitation forming the pulsating aurora may be accompanied by precipitation of relativistic electrons (Miyoshi et al., 2020; Shumko et al., 2021), which makes such a quasi-periodic precipitation pattern particularly important in the context of energetic electron losses and altering of atmosphere properties (Miyoshi et al., 2021). Incoherent scatter radar and ionospheric total electron content also show that ULF-modulated precipitation can significantly alter ionospheric conductance, potentially affecting the dynamics of a range of magnetosphere-ionosphere current systems and ULF waves (e.g., Buchert et al., 1999; Pilipenko, Belakhovsky, Kozlovsky, et al., 2014; Pilipenko, Belakhovsky, Murr, et al., 2014; Wang et al., 2020). Using ground-based ULF and equatorial whistler wave observations to characterize precipitation can at most confirm the temporal periodicity of its equatorial source, but cannot resolve the spatial periodicity of the precipitation nor the spatial periodicity of its equatorial sources. The most promising way to reveal both the temporal and spatial scales of electron precipitation patterns is to combine low-altitude, near-equatorial, and ground-based measurements.

In this study we analyze three events of quasi-periodic electron precipitation driven by near-equatorial electron scattering due to whistler-mode waves modulated by compressional ULF waves. We combine ground-based magnetometer (GMAG) measurements of ULF waves, low-altitude Electron Losses and Fields Investigation (ELFIN)-A and -B (Angelopoulos et al., 2020) measurements of >50 keV electron precipitation, and near-equatorial Time History of Events and Macroscale Interactions during Substorms (THEMIS; Angelopoulos, 2008) measurements of whistler-mode and ULF waves. Ground-based measurements localize the L-shell and magnetic local time (MLT) sector of ULF waves during the entire interval. Multi-spacecraft THEMIS measurements provide us with estimates of ULF wavelength (spatial scale), which serve as a good proxy for the spatial periodicity scale of whistler-mode wave modulation. Low-altitude ELFIN measurements of quasi-periodic electron precipitation show a spatial periodicity similar to the estimated ULF wavelength. Finally, the combination of near-equatorial measurements of whistler-mode wave characteristics and background plasma properties provides typical resonant energies of precipitating electrons, which agree well with the precipitating energy spectra in ELFIN measurements. In summary, these three selected events confirm that compressional ULF waves can modulate whistler-mode waves and result in spatially quasi-periodic precipitation of energetic electrons over a large L-shell and MLT domain.

The paper is organized as follows: in Section 2 we describe available data sets and methods of data analysis; in Section 3 we describe three events with combined ground-based, THEMIS, and ELFIN measurements; and in Section 4 we discuss our results and their possible application in radiation belt modeling.

# 2. Spacecraft Instruments and Data Set

Investigation of electron precipitation requires pitch-angle and energy resolved electron distributions within the loss cone, which is almost impossible near the equator due to the small loss cone size there (see, e.g., Kasahara et al., 2018). However, the much larger loss cone size at low altitudes allows polar-orbiting ionospheric space-craft to measure trapped and precipitating (those within the loss cone) electron fluxes. In this study, we employ energetic (>50 keV) electron precipitation measurements by the low-altitude (~450 km) twin ELFIN CubeSats (ELFIN-A and ELFIN-B), which provide electron pitch-angle distributions between 50 keV and 6 MeV, with energy resolution <40%, angular resolution of ~22.5° and temporal resolution of 2.8s (spin period) (Angelopoulos et al., 2020). We use the ratio of  $j_{loss}$  (pitch-angle-averaged flux within the loss cone) to  $j_{trap}$  (pitch-angle-averaged flux outside the loss cone) to study enhancements of precipitation driven by near-equatorial scattering of energetic electrons by whistler waves (see detailed analysis of ELFIN measurements of whistler-driven precipitation events in Artemyev et al. (2021), Mourenas et al. (2022), Tsai et al. (2022), and Zhang, Artemyev, et al. (2022)).

ELFIN measurements of  $j_{loss}/j_{trap}$  are supplemented by ULF wave observations from the THEMIS GMAG network (Russell et al., 2008; FYKN, BRW), U.S. Geological Survey's Geomagnetism Program magnetometer network (CMO, SHU), AUTUMNX magnetometer network (PUVR), and University of Iceland magnetometer (LRV). The main advantage of ground-based observations is the absence of spatio-temporal ambiguity inherent in spacecraft measurements. ELFIN flux ratio  $j_{loss}/j_{trap}$  measurements and ground-based ULF observations will be compared with equatorial THEMIS (Angelopoulos et al., 2008) measurements of ULF and very low frequency (whistler-mode frequency range) fields. The THEMIS fluxgate magnetometer (FGM; Auster et al., 2008)

SHI ET AL. 2 of 12

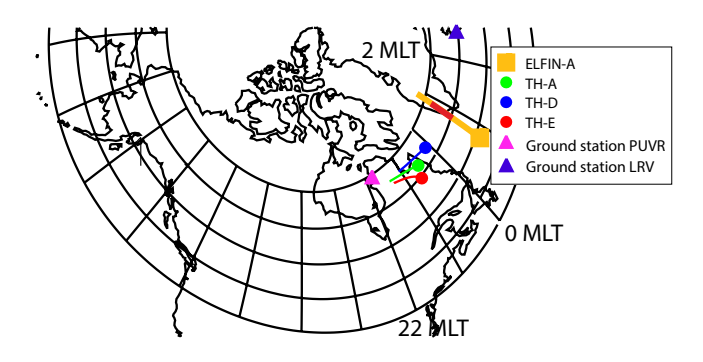


**Figure 1.** Projection of Electron Losses and Fields Investigation (ELFIN)-A orbits and Time History of Events and Macroscale Interactions during Substorms orbits to the ground, and the location of two ground stations on 17 June 2021, from 03:30 UT to 06:00 UT. The red trace along ELFIN-A orbit shows the sub-interval (05:32:30 UT to 05:33:30 UT) analyzed in Figure 3. The dots mark the start time of each orbit.

provides magnetic field with a 1/128, 1/4 or 3 s (spin period) sample rate (depending on availability and choice of data product), whereas the THEMIS search-coil magnetometer (SCM; Le Contel et al., 2008) provides <8 kHz waveform measurements that are further converted to on-board processed, Fast-mode Fast Fourier series, "FFF", spectra data over 32 or 64 frequency bands (Cully et al., 2008).

# 3. Analysis of Selected Events

We select three quasi-periodic precipitation events at ELFIN, which are in good conjunction with THEMIS, providing equatorial measurements of ULF and whistler waves, and with ground-based magnetometers providing measurements of ULF waves. We show detailed analysis of the first event, and then reinforce the conclusions using the two other events.

#### 3.1. Event #1

The first event happened on 17 June 2021. Figure 1 shows the projections of THEMIS (three spacecraft, TH-A, TH-D, and TH-E) orbits from 03:30 UT to

06:00 UT, and the projection of ELFIN-A orbits from 05:32:30 UT to 05:33:30 UT. We also include two ground stations (PUVR and LRV) located near the ELFIN-A (EL-A) and THEMIS footpoints.

Figures 2a-2c show the wavelet analysis of the ULF magnetic field component observed by THEMIS-E and two ground stations: the parallel (compressional) component is shown for THEMIS observations, and the East-West component (corresponding to poloidal oscillations in space) for the ground stations. The ground stations and THEMIS-E observed compressional ULF waves with similar frequency ranges, indicating that the same ULF waves existed over a large MLT (22-03) and L-shell  $\in$  [6, 9] domain (L shells here are calculated using the T89 model (Tsyganenko, 1989). During this event, THEMIS-E was in fast survey mode (when FFF data is available) and SCM measured quasi-periodic whistler wave bursts from 03:30 UT to 04:30 UT at L  $\sim$  6-9 (see Panel (d)). Within the same L-shell range, THEMIS-A and -D also observed similar whistler wave bursts (not shown here), consistent with expectation from the ground stations that the periodic whistler emission extended over a wide MLT range in space. Panel (e) shows the THEMIS-E whistler wave spectrum (in color) and the line-plot (black trace) of the field-aligned magnetic field component variation ( $\delta B_{-} = \delta B_{\parallel}$ ) of ULF waves between ~9–12 mHz. ULF waves in this frequency range are visible in THEMIS-E, consistent with the wave-power in the ground-based station measurements (see Panels (a-c)). Figure S1 in Supporting Information S1 further shows that ULF waves indeed form a local maximum in the frequency range consistent with the whistler-mode wave modulation frequency, that is, despite that the ULF wave spectrum is much broader, the part that modulates the whistler-mode waves remains clearly distinguishable from its entire spectrum. There is a reasonably good correlation of whistler wave bursts and local  $\delta B_{\parallel}$  minima (see expanded view of Panel (e) in Panel (g)). These observations are consistent with a scenario of a ULF-wave modulated thermal electron anisotropy, resulting in the observed quasi-periodic generation of whistler waves (as previously reported by W. Li, Bortnik, et al., 2011; L. Li et al., 2022; Xia et al., 2020; Zhang et al., 2019). Note the adiabatic effect of ULF waves (i.e., betatron heating/cooling) on electron distributions would reduce the electron anisotropy around the local plasma density enhancements (magnetic field minima), and thus will not generate strong whistler-mode waves (see discussion in Watt et al., 2011). However, compressional ULF waves may transport the transversely anisotropic electron population trapped within local magnetic field minima (density maxima), and such trapped population will be a primary source of whistler-mode wave generation (see discussion in Zhang et al., 2019). Although we mostly rely on the latter scenario in our explanation of ULF-modulated whistler-mode waves and electron precipitations, alternative or supplementary scenarios (e.g., W. Li, Bortnik, et al., 2011; W. Li, Thorne, Bortnik, Nishimura, & Angelopoulos, 2011; Rae et al., 2018; Watt et al., 2011) of ULF-modulated precipitations should also work for explanation of quasi-periodic precipitation observed by ELFIN.

SHI ET AL. 3 of 12

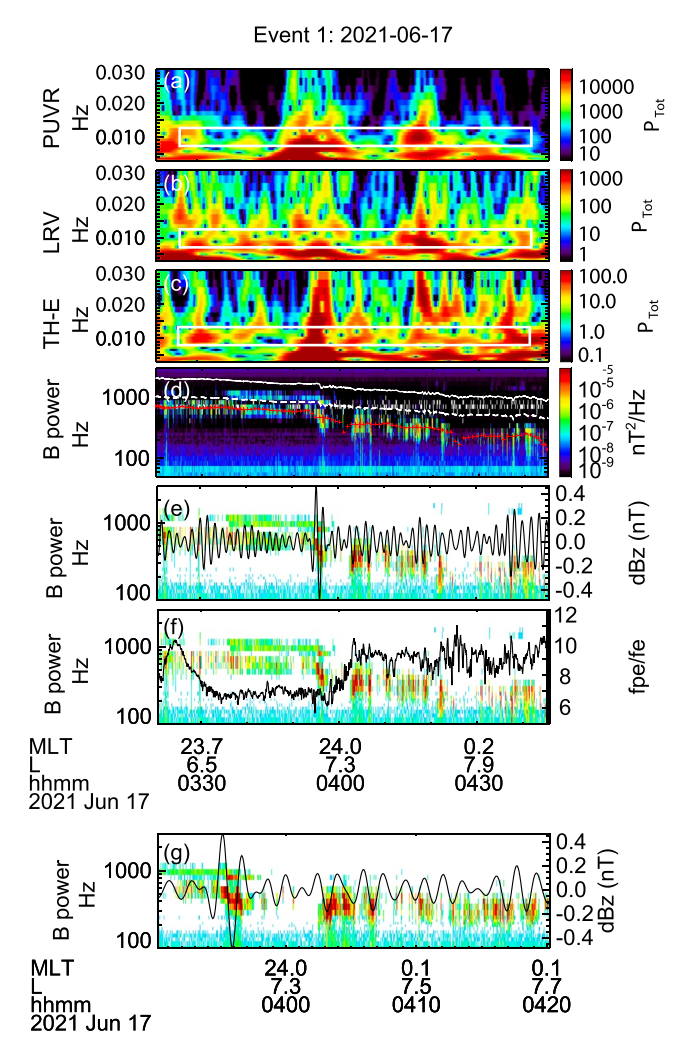


**Figure 2.** Observations of ultra-low-frequency (ULF) and whistler waves. Wavelet power spectra of the East-West component magnetic field at two ground stations (Panels a and b) and of the parallel magnetic field component at TH-E (Panels c and d, covering the ULF and very low frequency (VLF) range respectively). Panels (a–c) also demarcate, in white rectangles, the ULF band and time range of enhanced magnetic field fluctuations of interest. Panel (d) denotes peak whistler wave power in red crosses at 1 min cadence. Over-plotted in solid and dashed lines are  $f_{\rm ce}$  and  $0.5f_{\rm ce}$ . Panels (e and f) show the same overview of the VLF waves at TH-E, containing the same information as Panel (d), except only showing intensities greater than  $10^{-7}$  nT²/Hz. Overplotted on them are the band-pass filtered waveforms of  $\delta B_{\parallel}$  of ~10 mHz ULF waves, and  $f_{\rm pe}f_{\rm ce}$ , respectively. Panel (g) is a zoomed-in view, in time, of Panel (e).

To determine the typical energies of electrons precipitated by the observed quasi-periodic whistler waves, we calculate the mean wave frequency  $\langle f \rangle$ , and the frequency width  $\Delta f$ , using the following equations:

$$\langle f \rangle = \frac{\int_{f_{lh}}^{f_{ce}/2} B_w^2(f) f df}{\int_{f_{lh}}^{f_{ce}/2} B_w^2(f) df}$$

$$\Delta f = \left(\frac{\int_{f_{lh}}^{f_{ce}/2} B_w^2(f) \left(f^2 - \langle f \rangle^2\right) df}{\int_{f_{lh}}^{f_{ce}/2} B_w^2(f) df}\right)^{1/2}$$

where  $B_w^2$  is the wave intensity at a specific frequency,  $f_{\rm lh}$  is the lower hybrid frequency, and  $f_{\rm ce}$  is the electron cyclotron frequency. Figure 2d shows that the mean wave frequency  $\langle f \rangle$  (depicted by the red crosses), is between 200 and 800 Hz (0.2–0.4  $f_{\rm ce}$ ) and decreases with increasing L-shell. We calculate the cyclotron resonance energy of electrons for field-aligned whistler waves at the estimated mean frequency,  $\langle f \rangle$ , and at the minimum frequency,  $f_{\rm min} = \langle f \rangle - \Delta f$ , using the equation (Kennel & Petschek, 1966):

$$E_{res} = \frac{B^2}{2\mu_0 n_e} \frac{f_{ce}}{f} \left( 1 - \frac{f}{f_{ce}} \right)^3$$

where B is the magnetic field strength, estimated using the T89 (Tsyganenko, 1989) model scaled at the equatorial field intensity from THEMIS-E measurements, and  $n_a$  is the electron density from THEMIS-E equatorial measurements assumed to be constant along magnetic field lines. As the resonance energy increases with latitude, it is important to constrain waves to a reasonable latitudinal extent:  $|\lambda| \sim 30^{\circ}$  is used here as derived from the empirical whistler wave model (see O. V. Agapitov, Mourenas, Artemyev, Mozer, Bonnell et al., 2018; Meredith et al., 2001; Meredith et al., 2003) at the MLT sector of our observations. The resultant resonance energies are in the range of ~50-300 keV, showing that the observed whistlers can provide scattering and lead to precipitation of electrons in this energy range. It is worth noting that for the observed  $f_{\rm pe}/f_{\rm ce} \sim 6$ –12, typical electromagnetic ion cyclotron (EMIC) waves can only lead to the loss of >1 MeV electrons (e.g., Kersten et al., 2014), and therefore precipitation of 100 s of keV electrons should be mostly attributed to scattering by whistler waves. We anticipate that the quasi-periodic whistler waves, modulated by ULF waves, will lead to quasi-periodic energetic electron precipitation.

To test this hypothesis, we examine ELFIN-A observations of precipitating electron fluxes  $j_{\rm loss}$ , trapped electron fluxes  $j_{\rm trap}$ , and their ratio  $j_{\rm loss}/j_{\rm trap}$  (Figure 3). At the same L-shell and MLT sector where THEMIS observed ULF-modulated whistler waves, ELFIN-A indeed captured quasi-periodic precipitation of ~50–200 keV electrons with average peaks of  $j_{\rm loss}/j_{\rm trap} \geq 0.3$ , indicative of fast scattering caused by whistler waves. Such a

precipitating-to-trapped flux ratio corresponds to the near-loss-cone pitch-angle diffusion rate  $D_{aa} \sim 10^{-4} \text{ s}^{-1}$  (W. Li et al., 2013; Mourenas et al., 2021). For the *L*-shell range and  $f_{pe}f_{ce}$  ratio from Figure 2 such diffusion rate corresponds to whistler-mode wave amplitudes at  $\in$  [50, 150]pT (see, e.g., Figures 14 and 21 in Ni et al., 2016). The whistler wave amplitudes measured by THEMIS during this interval agree well with this range (see more examples of comparison of ELFIN precipitation rates and equatorial whistler-mode wave intensity measurements in Tsai et al., 2022; Mourenas et al., 2022). Note that moving along a low-altitude orbit, ELFIN crosses the entire *L*-shell range of precipitation within a couple of minutes, and thus the periodicity at ELFIN observations represents a spatial periodicity of the scattering process at and near the equator.

SHI ET AL. 4 of 12

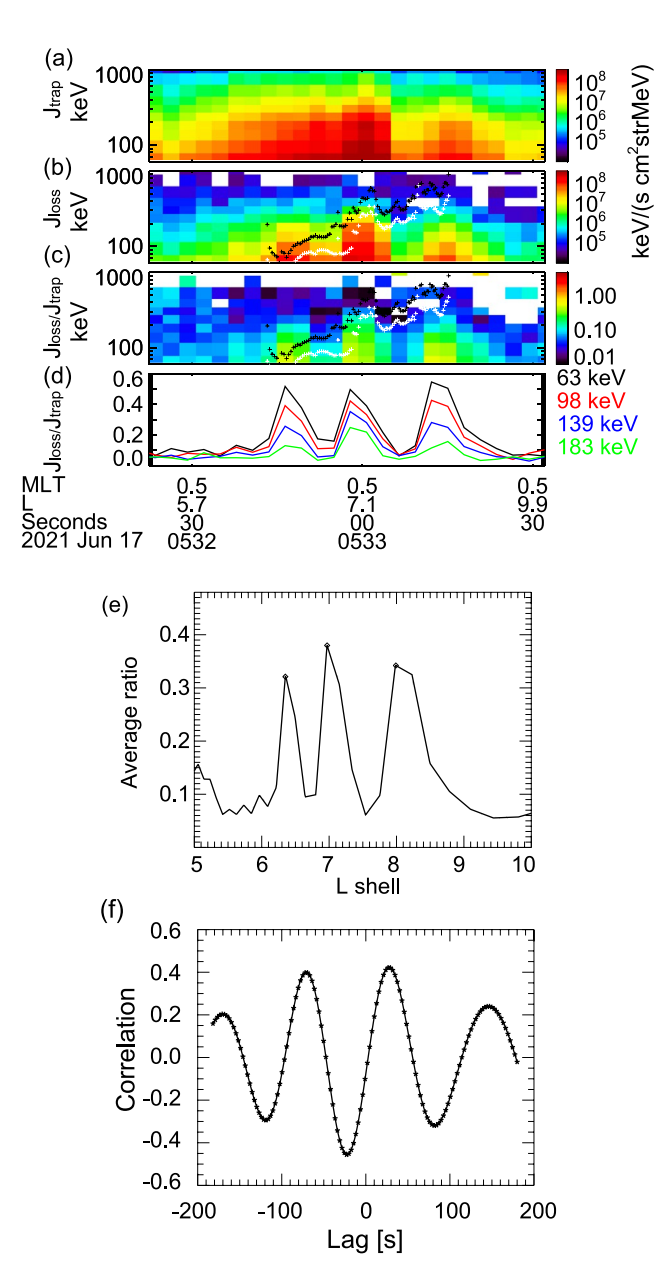


**Figure 3.** Electron Losses and Fields Investigation-observed trapped electron flux  $j_{\text{trap}}$  (a), precipitating flux  $j_{\text{loss}}$  (b), and the ratio  $j_{\text{loss}}/j_{\text{trap}}$  (c and d, in spectral- and line-plot format respectively). Black and white crosses in Panels (b and c) show the upper and mean resonance energy of the observed whistler waves (see text for details). (e) The average  $j_{\text{loss}}/j_{\text{trap}}$  of the first four energy channels. (f) Cross-correlation between the ultra-low-frequency wave field from Time History of Events and Macroscale Interactions during Substorms-A (THEMIS-A) and THEMIS-E as a function of lag time.

It is evident that these periodic  $j_{\rm loss}/j_{\rm trap}$  peaks contribute to most of the precipitating flux observed by ELFIN at L=6–9. This indicates that such periodic precipitation can play a major role in energetic electron losses during intervals with ULF-modulated whistler bursts. The highest energy channel showing the periodic  $j_{\rm loss}/j_{\rm trap}$  peaks is around 200 keV (Figure 3), located in Figures 3b and 3c between the upper (black crosses) and mean (white crosses) resonance energies corresponding to  $\langle f \rangle$  and  $f_{\rm min}$ , respectively. Thus, ELFIN measurements confirm that quasi-periodic whistler wave bursts observed by THEMIS are indeed responsible for quasi-periodic electron precipitation.

However, the periodicity seen by THEMIS is temporal, whereas the periodicity seen by ELFIN is spatial. ULF waves observed by THEMIS extend over a large L-shell and MLT sector (as revealed by ground-based observations), and thus ELFIN likely measures precipitation from spatially periodic whistler bursts with the periodicity comparable to ULF wavelengths. To confirm this, we compare the spatial scale of periodic precipitation peaks  $(\delta L)$  and our estimate of ULF wavelengths  $\delta \lambda$ . ELFIN moves along its orbit at a nearly constant geomagnetic longitude. Therefore, when mapped to the equator, ELFIN's trajectory, and the measured quasi-periodic precipitation, correspond approximately to a radial sampling of the equatorial magnetosphere. The spatial periodicity ( $\delta L$ ) of the precipitation can be estimated by calculating the spatial separations between the peaks of  $j_{loss}/j_{trap}$ . For three observed  $j_{\rm loss}/j_{\rm trap}$  peaks, the average spatial scale is 0.85  $\pm$  0.28 $R_E$ (Figure 3e, where ELFIN time-series of precipitation were converted to L-shell profiles of precipitation using the T89 model). If the precipitation is driven by ULF-modulated whistler waves, then this  $\delta L$  should be comparable to the ULF wavelength  $\delta\lambda$  in the radial direction (or, more precisely, the ULF field  $\delta B_{\parallel}$  periodicity in the radial direction). The wavelength in the radial direction can be calculated by using cross-correlation analysis on the ULF fields measured from two THEMIS spacecraft at similar MLT (mostly separated in the radial direction) to obtain the phase difference for the ULF wave. If the two spacecraft are radially separated by a distance r, and  $\delta B_{\parallel}$ (at a particular frequency f) at the two spacecraft has a phase difference  $\delta \phi$ . then the wavelength can be estimated as  $\lambda/2\pi = r/\delta\phi$ . The phase difference between two spacecraft can be calculated using  $\delta \phi = 2\pi \delta t/T$ , where  $\delta t$  is the lag time as inferred from the peak cross-correlation between the ULF wave field measured at the two spacecraft and T is the period of the wave. We use THEMIS-A and THEMIS-E measurements separated mostly along the radial direction over distances comparable with the expected ULF wavelength. We examined the phase difference of 9-12 mHz ULF waves between THEMIS-A and THEMIS-E (the radial distance is  $0.21R_{\rm p}$ ); Figure 3f shows that the cross-correlation peaks at a lag time of  $\delta t \sim 26.5$  s (the comparison of observed ULF waveforms is shown in Supporting Information S1). The corresponding wavelength is  $\delta \lambda \sim 0.78 R_E$ , which is very close to the  $\delta L \approx 0.85 \pm 0.28 R_E$  derived above from ELFIN measurements. These spatial dimensions are consistent with past studies of ULF-induced precipitation (e.g., Baddeley et al., 2017), and provide further support for the idea that the periodic precipitation is driven by ULF-modulated periodic whistler waves.

#### 3.2. Event #2

The second conjunction event occurred on 13 May 2021. Figure 4 shows the orbit projections of THEMIS-A, -D, and -E in the northern hemisphere from 17:00 UT to 19:00 UT, and the ELFIN-B orbit projection from 17:12 UT to 17:15 UT. Two ground stations (BRW and FYKN) were located near the ELFIN-B and THEMIS footpoints at the time. The ground stations and three THEMIS spacecraft observed ULF waves over a similar frequency

SHI ET AL. 5 of 12

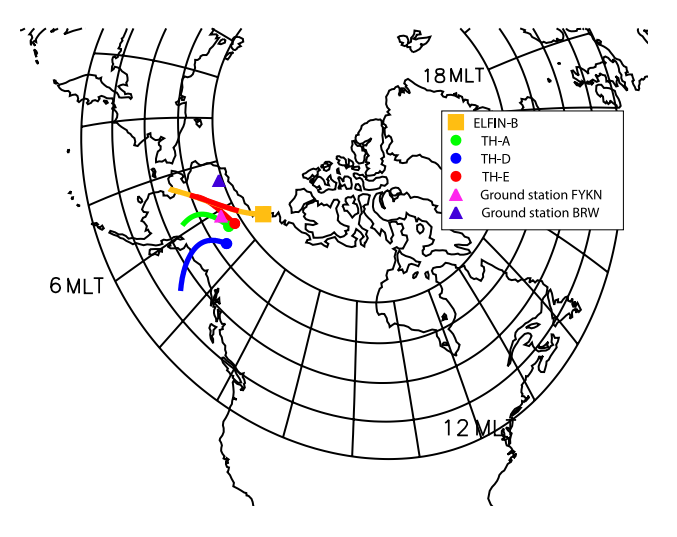


**Figure 4.** Projection of Electron Losses and Fields Investigation (ELFIN)-B and Time History of Events and Macroscale Interactions during Substorms orbits to the ground, and the location of two ground stations on 13 May 2021, from 17:00 UT to 19:00 UT. The red trace along ELFIN-B's orbit shows the sub-interval (17:12:30 UT to 17:14:40 UT) analyzed in Figure 5. The dots mark the start time of each orbit.

range (Figures 5a–5c). We are mostly interested in ULF waves from 3 to 5 mHz (depicted by the rectangle in Figure 5c), because THEMIS-E observed quasi-periodic whistler wave bursts (from 17:00 UT to 19:00 UT, see Figure 5d) modulated at a frequency ~4 mHz; see Figure 5e for the correlation of the peaks of whistler wave intensity and  $\delta B_{\parallel}$  of compressional ULF wave component band-pass filtered at 3 – 5 mHz (see Figure S1 in Supporting Information S1 for comparisons of the ULF spectrum and spectrum of the whistler-mode wave intensity). The whistler waves' mean frequency increases from 150 to 700 Hz (0.1–0.2  $f_{\rm ce}$ ) as THEMIS-E moves to lower L-shells. Such whistler waves can resonate with ~50–1,000 keV electrons for the observed  $f_{\rm pe}/f_{\rm ce}$  ~ 6–20 (see Figure 5f). Note that for such a low  $f_{\rm pe}/f_{\rm ce}$ , we can ignore the contribution of EMIC waves to the scattering of  $\lesssim$ 1 MeV electrons (Summers et al., 2007).

Around 17:13 UT, ELFIN-B traversed the same *L*-shell and MLT region where THEMIS captured quasi-periodic whistler waves. ELFIN-B observed strong bursts of electron precipitation with the precipitating to trapped flux ratio reaching (or even slightly exceeding) one for 10-100 s of keV electrons (see Figures 5h–5i). The periodic peaks of  $j_{loss}/j_{trap}$  are observed up to ~500–600 keV. As in the previous event studied, this energy range is consistent with the resonance energies of electrons for the observed whistler waves (with an assumption of wave propagation up to ~30° of magnetic latitude; the typical latitudinal spread of whistler waves at this MLT sector, see O. V. Agapitov, Mourenas, Artemyev, Mozer, Bonnell et al., 2018; Mereditin

et al., 2001; Meredith et al., 2003). Within the quasi-periodic precipitation, ELFIN also observed spin-resolution bursts with  $j_{loss}/j_{trap} \ge 1$  up to 600 keV, around the mean resonance energies estimated for THEMIS measurements of whistler waves and background plasma. These are likely very short, microburst-like precipitation lasting less than one spin of ELFIN (see detailed analysis of such microbursts observed by ELFIN in Zhang, Angelopoulos, et al. (2022)). Miyoshi et al. (2020) and Shumko et al. (2021) previously reported that relativistic microbursts may be embedded into quasi-periodic precipitation of low-energy (<50 keV) electrons. Our observations of strong precipitation at the minimum detectable energy ( $\approx$ 50 keV), are suggestive that precipitation extends to <50 keV and support the idea that <50 and >500 keV losses can occur simultaneously. Furthermore they indicate that such broad energy precipitation can occur during ULF-driven, quasi-periodic precipitation.

Figure 5k marks the local precipitation maxima (peaks) in the plot of  $j_{loss}/j_{trap}$  as a function of L. Only peaks with  $j_{loss}/j_{trap} > 0.3$  have been considered. The spatial periodicity of these peaks is  $\delta L = 0.5 \pm 0.17 R_E$ . The phase difference of 3–5 mHz ULF waves between THEMIS-A and THEMIS-E using the method described for Event #1 (see Figure S2b in Supporting Information S1) results in an inferred equatorial ULF wavelength of  $0.62R_E$ , approximately in the radial direction, which is close to the  $\delta L$  derived from ELFIN measurements.

# 3.3. Event #3

The third event occurred on 22 October 2021. Figure 6 shows the orbit projections of THEMIS from 10:00 UT to 12:00 UT and the ELFIN-A orbit projection from 11:48 UT to 11:51 UT. THEMIS-E observed quasi-periodic whistler waves modulated by 10–20 mHz compressional ULF waves during 10:20 UT to 10:50 UT (Figure 7c). For this event, THEMIS and ELFIN footpoints in the north hemisphere are located near MLT = 23. No ground-based stations are available in the same MLT, however, ground-based stations (SHU and CMO) at MLT = 0 – 1 detected the same, 10–20 mHz frequency ULF wave Figures 7a and 7b), therefore the ULF waves covered a large MLT, L-shell domain. ELFIN-A observed quasi-periodic electron precipitation within  $L \in [5.5, 7.5]$  (corresponding to whistler wave bursts observed by THEMIS) with  $\delta L = 0.33 \pm 0.045$  ( $\delta L$  is the average spatial scale between the precipitation peaks shown in Figure 7k). The precipitating to trapped flux ratio of 10–100 s of keV electrons exhibits peaks at around 0.1–0.3. The highest energy channel showing the periodic peaks, ~300 keV, is between the upper and mean resonance energies estimated for THEMIS measurements of whistler waves using the local plasma density (assumed to be the same as at the equator). The wavelength of the 10–20 mHz ULF waves (estimated by comparing THEMIS-A and THEMIS-E ULF measurements) is  $\delta \lambda \sim 0.27 R_E$  (the ULF fields are shown

SHI ET AL. 6 of 12

21699402, 2022, 12, Downloaded from https://agupubs.onlinelibrary.wiley.com/doi/10.1029/2022JA030932 by University of California - Los Ange, Wiley Online Library on [25/07/2023]. See the Terms and Conditions



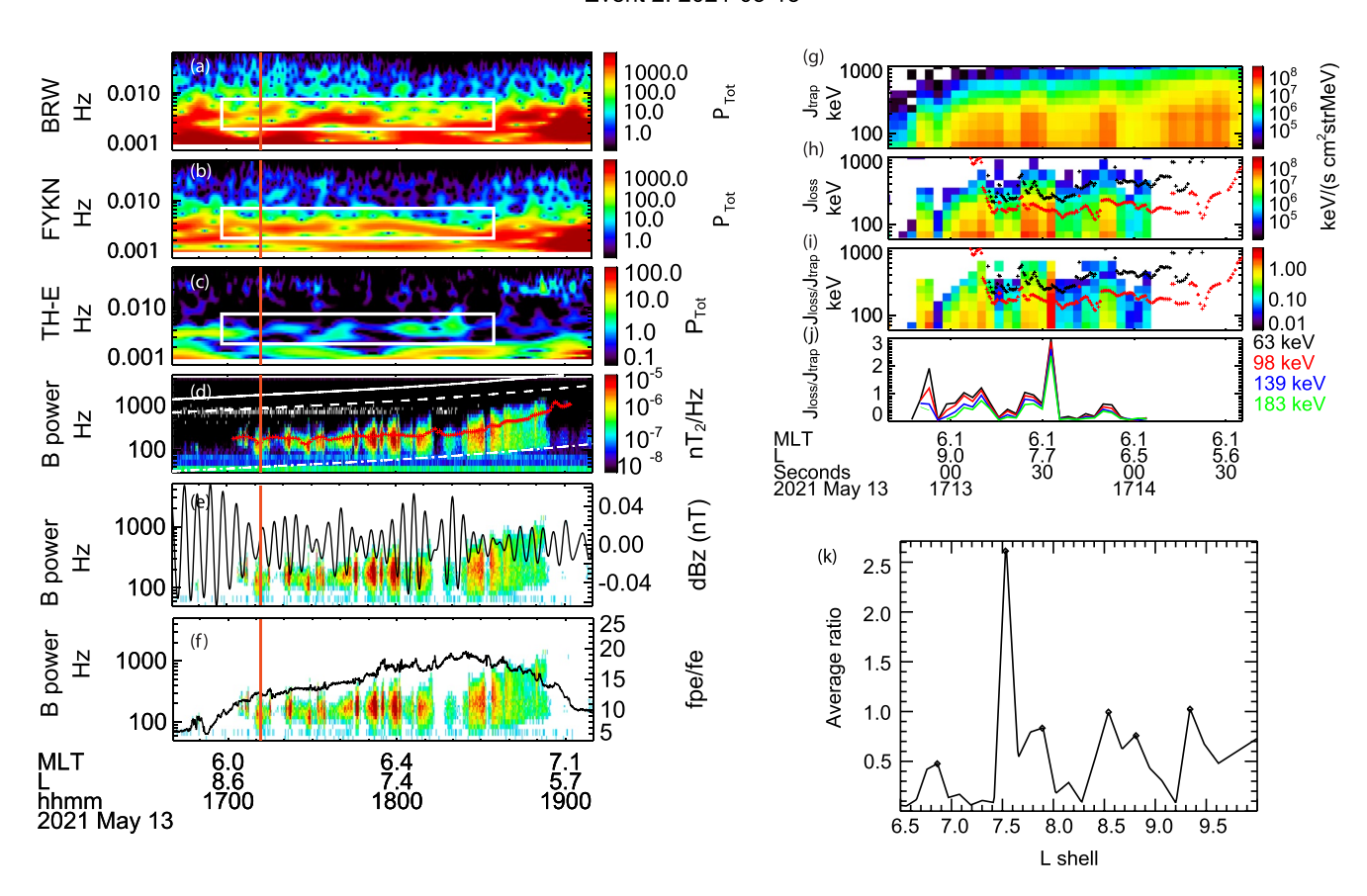


Figure 5. Observations of ultra-low-frequency (ULF) and whistler waves. East-West component magnetic field at two ground stations (Panels a and b) and of the parallel magnetic field component at TH-E (Panels c and d, covering the ULF and very low frequency (VLF) range respectively). Panels (a–c) also demarcate, in white rectangles, the ULF band and time range of enhanced magnetic field fluctuations of interest. Panel (d) denotes peak whistler wave power in red crosses at 1 min cadence. Over-plotted in solid, dashed, and dashed-dotted lines are  $f_{ce}$ ,  $0.5f_{ce}$ , and  $f_{lh}$ , respectively. Panels (e and f) show the same overview of the VLF waves at TH-E, containing the same information as Panel (d), except only showing intensities greater than  $10^{-7}$  nT<sup>2</sup>/Hz. Overploted on them are the band-pass filtered waveforms of  $\delta B_{\parallel}$  of ~4 mHz ULF waves, and  $f_{p_e}/f_{ce}$ , respectively. The vertical red line indicates the time of Electron Losses and Fields Investigation (ELFIN)-B pass. Panels (g–i) show ELFIN observations of trapped electron flux  $j_{trap}$ , precipitating flux  $j_{loss}$ , and the ratio  $j_{loss}/j_{trap}$ , respectively. Black and red crosses show the upper and mean resonance energy of whistler waves. Panel (j) is the same information as Panel (i) except only for the four lowest energies, with the ratios depicted as line-plots. Panel (k) is the average  $j_{loss}/j_{trap}$  of the first four energy channels.

in Figure S2c in Supporting Information S1), consistent with the spatial periodicity of electron precipitation. Both Events #2 and #3 support the hypothesis that the ULF-modulated periodic whistler waves lead to the observed periodic precipitation.

# 4. Discussion and Conclusions

Compressional ULF waves are known to modulate equatorial electron populations causing whistler-mode wave generation (W. Li, Thorne, Bortnik, Nishimura, & Angelopoulos, 2011; Watt et al., 2011; Xia et al., 2016, 2020; Zhang et al., 2019), resulting quasi-periodic electron precipitation (Kasahara et al., 2018; Nishimura et al., 2010). Such precipitation is not only modulated by ULF waves but actually generated by such waves: the ULF waves can drive marginally unstable plasmas of the inner magnetosphere to whistler-mode instability which can cause subsequent electron precipitation (Xia et al., 2016; Zhang et al., 2019). The subject ULF waves are typically generated at the magnetopause by solar wind transients and propagate toward the inner magnetosphere (e.g., O. V. Agapitov et al., 2009; Hartinger et al., 2013, 2014; Hwang & Sibeck, 2016). Both the ULF waves (Di Matteo et al., 2022; Elsden et al., 2022; Klimushkin et al., 2019; Wright & Elsden, 2020) and the correlated whistler-mode waves (Zhang et al., 2020) have been observed to extend over a large *L*-shell and MLT range. However, the effi-

SHI ET AL. 7 of 12

21699402, 2022, 12, Downloaded from https://agupubs.onlinelibrary.wiley.com/doi/10.1029/2021A039932 by University of California - Los Ange, Wiley Online Library on [2507/2023]. See the Terms and Conditions (thps://onlinelibrary.wiley.com/terms-ad-conditions) on Wiley Online Library for rules of use; O.A articles are governed by the applicable Creat

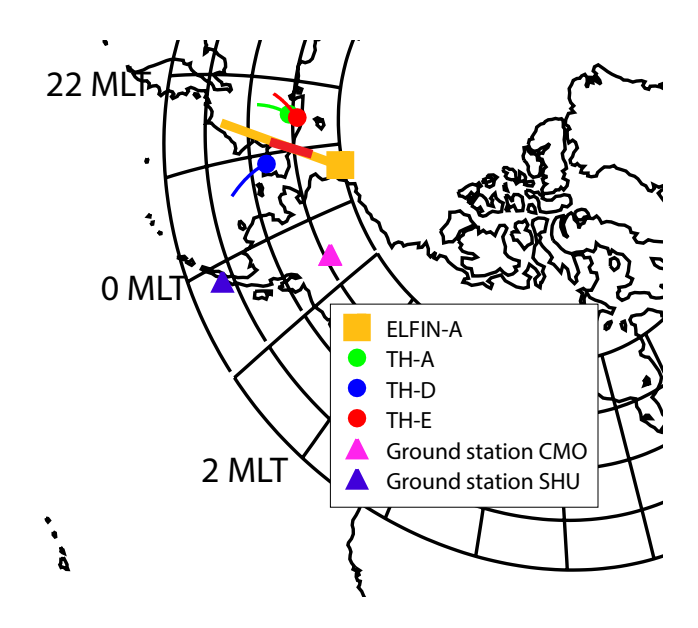


**Figure 6.** Projection of Electron Losses and Fields Investigation (ELFIN)-A orbits and Time History of Events and Macroscale Interactions during Substorms orbits to the ground, and the location of two ground stations on 22 October 2021, from 10:20 UT to 10:50 UT. The red trace along the ELFIN-A orbit projection shows the sub-interval (11:48:50 UT to 11:49:40 UT) analyzed in Figure 7. The symbols mark the start time of each orbit.

## Event 3: 2021-10-22

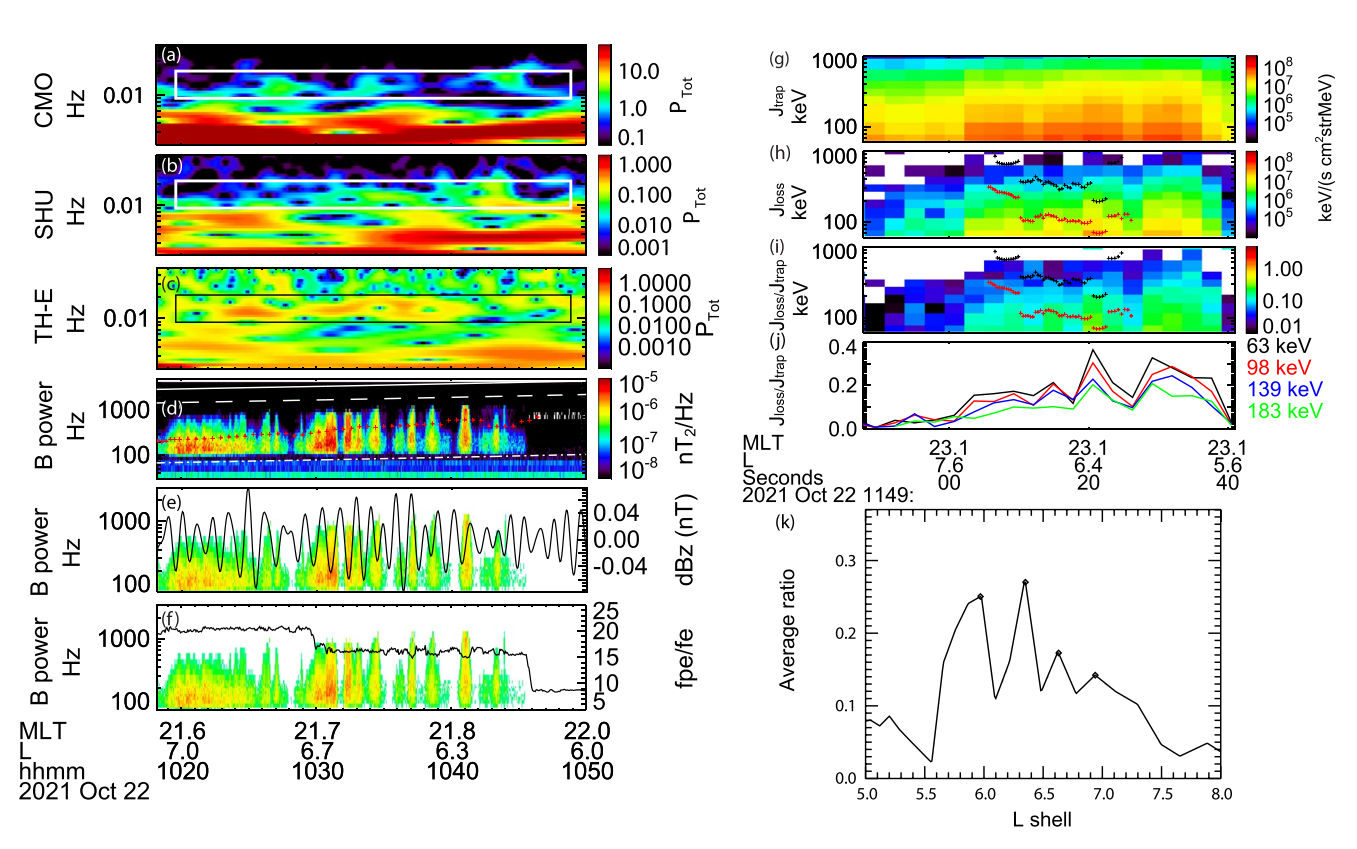


Figure 7. Ultra-low-frequency wavelet spectra at two ground stations and Time History of Events and Macroscale Interactions during Substorms-E (THEMIS-E), spectra of whistler waves at THEMIS-E, and electron precipitation observed at Electron Losses and Fields Investigation-A, in the same format as Figure 5.

SHI ET AL. 8 of 12

ciency of electron precipitation by such ULF-driven whistler-mode waves (e.g., the precipitating electron energy range, flux magnitude and net contribution to the ionospheric energy input) cannot be reliably determined from equatorial spacecraft measurements alone. In this study we use low-altitude observations of such precipitation in conjunction with ground based and equatorial measurements of the ULF and whistler waves to show that during three events:

- Electron precipitation exhibits spatial periodicity (in L-shell) with a scale comparable to that of equatorial ULF wavelengths. ULF waves and the associated whistler-mode wave driven precipitation extend over L-shells from the plasmasphere to the magnetopause (in agreement with Sandhu et al. (2021), Wright and Elsden (2020), and Zhang et al. (2020)). ULF waves cause spatially and temporally periodic modulations of whistler-mode waves, and lead to the subsequent periodic scattering of energetic electrons across a wide L-shell region. Such modulated scattering and precipitation are expected over the entire MLT region where compressional ULF waves are sufficiently intense to modulate whistlers.
- The energy of the precipitating electrons can range from below the low energy limit of the ELFIN instrument (50 keV) to upwards of 100 keV, to as high as ~1 MeV. The upward limit is consistent with the estimated maximum resonance energy of the observed whistler-mode waves, for the observed equatorial plasma conditions, and empirical constraints on the wave distribution along magnetic field lines (see O. V. Agapitov, Mourenas, Artemyev, Mozer, Bonnell et al., 2018). This energy range of precipitation covers the entire radiation belt "seed" electron population, and extends upwards into the low-energy portion of radiation belt electrons (Boyd et al., 2018; Jaynes, Baker, et al., 2015; Turner et al., 2021).
- The observed quasi-periodic precipitation of ~500 keV-1 MeV electrons which is squarely attributed to quasi-periodic whistler-mode waves, can only be the result of resonance at middle to high magnetic latitudes (where the local  $f_{pe}/f_{ce}$  can be sufficiently low). For the waves to propagate to such high latitudes (along the field line) without becoming oblique and Landau-damped by the thermal electrons, it must be that they are ducted (see discussion in Artemyev et al., 2021) by plasma density gradients (e.g., Chen et al., 2021; Hanzelka & Santolík, 2019; Streltsov & Bengtson, 2020). The ducts themselves must be also be set up by the compressional character of the ULF waves, since the observed relativistic electron precipitation exhibits the spatial structure of the ULF waves.

These results confirm the important role of ULF waves in precipitating not only auroral (<10 keV) electrons (Kasahara et al., 2018; Nishimura et al., 2010), but also energetic (~100 keV) and even relativistic (>500 keV) electrons. Therefore, whistler-mode waves generated by ULF-modulated thermal electron anisotropy can contribute significantly to radiation belt dynamics. The generation of whistler-mode waves by ULF-wave modulation of the plasma sheet electrons is very different from the classical mechanism of whistler-mode wave generation by electron injections during substorms (e.g., Fu et al., 2014; Tao et al., 2011; Thorne et al., 2010). Thus, the electron precipitation discussed herein does not necessary coincide with geomagnetic activity associated with substorms (identified using auroral electrojet indices AE and AL). Such a mechanism of energetic electron precipitation during instantaneously low AE intervals can still significantly deplete the remnant radiation belts that may have been built up by prior activity. Yet, this mechanism may be underestimated or completely absent in models of inner magnetosphere dynamics and magnetosphere-ionosphere coupling. While ULF waves can also be generated by substorm-time injections (e.g., Liu et al., 2017; Runov et al., 2014), magnetopause buffeting by solar wind pressure variations and by ion foreshock transients (e.g., Hartinger et al., 2013; Hartinger et al., 2014; Hwang & Sibeck, 2016) is thought to result in the largest amplitude ULF waves (e.g., Di Matteo et al., 2022). Examination of a wider variety of events using the methods presented herein can determine how the spatial scale of ULF-modulated precipitation varies according to the ULF wave driver. Future parameterization of ULF-driven whistler-mode waves and inclusion of this wave population in radiation belt models can improve our understanding of solar wind transients as a driver of electron precipitation, through ULF wave generation at the dayside magnetopause and subsequent whistler wave generation as ULF waves propagate inward as well as toward the flanks.

# **Data Availability Statement**

ELFIN data is available at https://data.elfin.ucla.edu/. THEMIS data is available at http://themis.ssl.berkeley.edu. Data was retrieved and analyzed using SPEDAS V4.1, see Angelopoulos et al. (2019).

SHI ET AL. 9 of 12

21699402, 2022, 12, Downloaded from https://agupub:

#### Acknowledgments

A.V.A., X.-J.Z. acknowledge support by NASA awards 80NSSC21K0729, 80NSSC19K0266, and 80NSSC22K0522, and A.V.A., X.-J.Z., and V.A. acknowledge support by NSF Grants AGS-1242918, AGS-2019950, and AGS-2021749. M.D.H. acknowledges support by NASA Grants 80NSSC21K1683 and 80NSSC19K0907. We are grateful to NASA's CubeSat Launch Initiative for ELFIN's successful launch in the desired orbits. We acknowledge early support of ELFIN project by the AFOSR, under its University Nanosat Program, UNP-8 project, contract FA9453-12-D-0285, and by the California Space Grant program. We acknowledge critical contributions of numerous volunteer ELFIN team student members. We acknowledge support by NSF Magnetospherics Base Program. We thank E. V. Masongsong for editorial assistance with the manuscript.

#### References

- Agapitov, O., Mourenas, D., Artemyev, A., Mozer, F. S., Bonnell, J. W., Angelopoulos, V., et al. (2018). Spatial extent and temporal correlation of chorus and hiss: Statistical results from multipoint THEMIS observations. *Journal of Geophysical Research: Space Physics*, 123(10), 8317–8330. https://doi.org/10.1029/2018JA025725
- Agapitov, O. V., Artemyev, A., Krasnoselskikh, V., Khotyaintsev, Y. V., Mourenas, D., Breuillard, H., et al. (2013). Statistics of whistler mode waves in the outer radiation belt: Cluster STAFF-SA measurements. *Journal of Geophysical Research*, 118(6), 3407–3420. https://doi.org/10.1002/jgra.50312
- Agapitov, O. V., Artemyev, A. V., Mourenas, D., Mozer, F. S., & Krasnoselskikh, V. (2015). Nonlinear local parallel acceleration of electrons through Landau trapping by oblique whistler mode waves in the outer radiation belt. *Geophysical Research Letters*, 42(23), 10. https://doi.org/10.1002/2015GL066887
- Agapitov, O. V., Blum, L. W., Mozer, F. S., Bonnell, J. W., & Wygant, J. (2017). Chorus whistler wave source scales as determined from multipoint Van Allen probe measurements. *Geophysical Research Letters*, 44(6), 2634–2642. https://doi.org/10.1002/2017GL072701
- Agapitov, O. V., Glassmeier, K.-H., Plaschke, F., Auster, H.-U., Constantinescu, D., Angelopoulos, V., et al. (2009). Surface waves and field line resonances: A THEMIS case study. *Journal of Geophysical Research*, 114(A1), A00C27. https://doi.org/10.1029/2008JA013553
- Agapitov, O. V., Mourenas, D., Artemyev, A. V., Mozer, F. S., Hospodarsky, G., Bonnell, J., & Krasnoselskikh, V. (2018b). Synthetic empirical chorus wave model from combined Van Allen probes and cluster statistics. *Journal of Geophysical Research: Space Physics*, 123(1), 297–314. https://doi.org/10.1002/2017JA024843
- Angelopoulos, V. (2008). The THEMIS mission. Space Science Reviews, 141(1-4), 5-34. https://doi.org/10.1007/s11214-008-9336-1
- Angelopoulos, V., Cruce, P., Drozdov, A., Grimes, E. W., Hatzigeorgiu, N., King, D. A., et al. (2019). The Space physics environment data analysis system (SPEDAS). Space Science Reviews, 215(1), 9. https://doi.org/10.1007/s11214-018-0576-4
- Angelopoulos, V., McFadden, J. P., Larson, D., Carlson, C. W., Mende, S. B., Frey, H., et al. (2008). Tail reconnection triggering substorm onset. Science, 321(5891), 931–935. https://doi.org/10.1126/science.1160495
- Angelopoulos, V., Tsai, E., Bingley, L., Shaffer, C., Turner, D. L., Runov, A., et al. (2020). The ELFIN mission. Space Science Reviews, 216(5), 103. https://doi.org/10.1007/s11214-020-00721-7
- Artemyev, A. V., Demekhov, A. G., Zhang, X. J., Angelopoulos, V., Mourenas, D., Fedorenko, Y. V., et al. (2021). Role of ducting in relativistic electron loss by whistler-mode wave scattering. *Journal of Geophysical Research: Space Physics*, 126(11), e29851. https://doi.org/10.1029/2021JA029851
- Auster, H. U., Glassmeier, K. H., Magnes, W., Aydogar, O., Baumjohann, W., Constantinescu, D., et al. (2008). The THEMIS fluxgate magnetometer. Space Science Reviews, 141(1-4), 235–264. https://doi.org/10.1007/s11214-008-9365-9
- Baddeley, L. J., Lorentzen, D. A., Partamies, N., Denig, M., Pilipenko, V. A., Oksavik, K., et al. (2017). Equatorward propagating auroral arcs driven by ULF wave activity: Multipoint ground- and space-based observations in the dusk sector auroral oval. *Journal of Geophysical Research: Space Physics*, 122(5), 5591–5605. https://doi.org/10.1002/2016JA023427
- Belon, A. E., Maggs, J. E., Davis, T. N., Mather, K. B., Glass, N. W., & Hughes, G. F. (1969). Conjugacy of visual auroras during magnetically quiet periods. *Journal of Geophysical Research*, 74(1), 1–28. https://doi.org/10.1029/JA074i001p00001
- Boyd, A. J., Turner, D. L., Reeves, G. D., Spence, H. E., Baker, D. N., & Blake, J. B. (2018). What causes radiation belt enhancements: A survey of the Van Allen probes era. *Geophysical Research Letters*, 45(11), 5253–5259. https://doi.org/10.1029/2018GL077699
- Breneman, A. W., Halford, A., Millan, R., McCarthy, M., Fennell, J., Sample, J., et al. (2015). Global-scale coherence modulation of radiation-belt electron loss from plasmaspheric hiss. *Nature*, 523(7559), 193–195. https://doi.org/10.1038/nature14515
- Bryant, D. A., Courtier, G. M., & Bennett, G. (1971). Equatorial modulation of electrons in a pulsating aurora. *Journal of Atmospheric and Terrestrial Physics*, 33(6), 859–867. https://doi.org/10.1016/0021-9169(71)90086-9
- Buchert, S. C., Fujii, R., & Glassmeier, K. H. (1999). Ionospheric conductivity modulation in ULF pulsations. *Journal of Geophysical Research*, 104(A5), 10119–10134. https://doi.org/10.1029/1998JA900180
- Capannolo, L., Li, W., Ma, Q., Shen, X. C., Zhang, X. J., Redmon, R. J., et al. (2019). Energetic electron precipitation: Multievent analysis of its spatial extent during EMIC wave activity. *Journal of Geophysical Research: Space Physics*, 124(4), 2466–2483. https://doi.org/10.1029/2018JA026291
- Chen, R., Gao, X., Lu, Q., Chen, L., Tsurutani, B. T., Li, W., & Wang, S. (2021). In situ observations of whistler mode chorus waves guided by density ducts. *Journal of Geophysical Research: Space Physics*, 126(4), e28814. https://doi.org/10.1029/2020JA028814
- Coroniti, F. V., & Kennel, C. F. (1970). Electron precipitation pulsations. *Journal of Geophysical Research*, 75(7), 1279–1289. https://doi.org/10.1029/JA075i007p01279
- Cully, C. M., Ergun, R. E., Stevens, K., Nammari, A., & Westfall, J. (2008). The THEMIS digital fields board. Space Science Reviews, 141(1–4), 343–355. https://doi.org/10.1007/s11214-008-9417-1
- Di Matteo, S., Villante, U., Viall, N., Kepko, L., & Wallace, S. (2022). On differentiating multiple types of ULF magnetospheric waves in response to solar wind periodic density structures. *Journal of Geophysical Research: Space Physics*, 127(3), e30144. https://doi.org/10.1029/2021JA030144
- Douma, E., Rodger, C. J., Blum, L. W., & Clilverd, M. A. (2017). Occurrence characteristics of relativistic electron microbursts from SAMPEX observations. *Journal of Geophysical Research: Space Physics*, 122(8), 8096–8107. https://doi.org/10.1002/2017JA024067
- Elsden, T., Yeoman, T. K., Wharton, S. J., Rae, I. J., Sandhu, J. K., Walach, M. T., et al. (2022). Modeling the varying location of field line resonances during geomagnetic storms. *Journal of Geophysical Research: Space Physics*, 127(1), e29804. https://doi.org/10.1029/2021JA029804
- Foster, J. C., Erickson, P. J., Baker, D. N., Claudepierre, S. G., Kletzing, C. A., Kurth, W., et al. (2014). Prompt energization of relativistic and highly relativistic electrons during a substorm interval: Van Allen probes observations. *Geophysical Research Letters*, 41(1), 20–25. https://doi.org/10.1002/2013GL058438
- Fu, X., Cowee, M. M., Friedel, R. H., Funsten, H. O., Gary, S. P., Hospodarsky, G. B., et al. (2014). Whistler anisotropy instabilities as the source of banded chorus: Van Allen probes observations and particle-in-cell simulations. *Journal of Geophysical Research: Space Physics*, 119(10), 8288–8298. https://doi.org/10.1002/2014JA020364
- Gan, L., Li, W., Ma, Q., Artemyev, A. V., & Albert, J. M. (2020). Unraveling the formation mechanism for the bursts of electron butterfly distributions: Test particle and quasilinear simulations. *Geophysical Research Letters*, 47(21), e90749. https://doi.org/10.1029/2020GL090749
- Hanzelka, M., & Santolík, O. (2019). Effects of ducting on whistler mode chorus or exohiss in the outer radiation belt. Geophysical Research Letters, 46(11), 5735–5745. https://doi.org/10.1029/2019GL083115
- Hartinger, M. D., Turner, D. L., Plaschke, F., Angelopoulos, V., & Singer, H. (2013). The role of transient ion foreshock phenomena in driving Pc5 ULF wave activity. *Journal of Geophysical Research*, 118(1), 299–312. https://doi.org/10.1029/2012JA018349

SHI ET AL. 10 of 12

- Hartinger, M. D., Welling, D., Viall, N. M., Moldwin, M. B., & Ridley, A. (2014). The effect of magnetopause motion on fast mode resonance. Journal of Geophysical Research, 119(10), 8212–8227. https://doi.org/10.1002/2014JA020401
- Hsieh, Y.-K., Omura, Y., & Kubota, Y. (2022). Energetic electron precipitation induced by oblique whistler mode chorus emissions. *Journal of Geophysical Research: Space Physics*, 127(1), e29583. https://doi.org/10.1029/2021JA029583
- Hwang, K. J., & Sibeck, D. G. (2016). Role of low-frequency boundary waves in the dynamics of the dayside magnetopause and the inner magneto-sphere. Washington DC American Geophysical Union Geophysical Monograph Series, 216, 213–239. https://doi.org/10.1002/9781119055006.ch13
- Jaynes, A. N., Baker, D. N., Singer, H. J., Rodriguez, J. V., Loto'aniu, T. M., Ali, A. F., et al. (2015a). Source and seed populations for relativistic electrons: Their roles in radiation belt changes. *Journal of Geophysical Research: Space Physics*, 120(9), 7240–7254. https://doi.org/10.1002/2015JA021234
- Jaynes, A. N., Lessard, M. R., Takahashi, K., Ali, A. F., Malaspina, D. M., Michell, R. G., et al. (2015b). Correlated Pc4-5 ULF waves, whistler-mode chorus, and pulsating aurora observed by the Van Allen probes and ground-based systems. *Journal of Geophysical Research*, 120(10), 8749–8761. https://doi.org/10.1002/2015JA021380
- Johnstone, A. D. (1978). Pulsating aurora. Nature, 274(5667), 119-126. https://doi.org/10.1038/274119a0
- Kasahara, S., Miyoshi, Y., Yokota, S., Kasahara, Y., Matsuda, S., Kumamoto, A., et al. (2018). Pulsating aurora from electron scattering by chorus waves. *Nature*, 554(7692), 337–340. https://doi.org/10.1038/nature25505
- Kennel, C. F., & Petschek, H. E. (1966). Limit on stably trapped particle fluxes. Journal of Geophysical Research, 71, 1–28. https://doi. org/10.1029/iz071i001p00001
- Kersten, T., Horne, R. B., Glauert, S. A., Meredith, N. P., Fraser, B. J., & Grew, R. S. (2014). Electron losses from the radiation belts caused by EMIC waves. *Journal of Geophysical Research*, 119(11), 8820–8837. https://doi.org/10.1002/2014JA020366
- Klimushkin, D. Y., Mager, P. N., Zong, Q., & Glassmeier, K.-H. (2019). Alfvén wave generation by a compact source moving on the magnet-opause: Asymptotic solution. *Journal of Geophysical Research: Space Physics*, 124(4), 2720–2735. https://doi.org/10.1029/2018JA025801
- Le Contel, O., Roux, A., Robert, P., Coillot, C., Bouabdellah, A., de La Porte, B., et al. (2008). First results of the THEMIS search coil magnetometers. Space Science Reviews, 141(1-4), 509-534. https://doi.org/10.1007/s11214-008-9371-y
- Li, L., Omura, Y., Zhou, X.-Z., Zong, Q.-G., Rankin, R., Yue, C., & Fu, S.-Y. (2022). Nonlinear wave growth analysis of chorus emissions modulated by ulf waves. *Geophysical Research Letters*, 49(10), e2022GL097978. https://doi.org/10.1029/2022GL097978
- Li, W., Bortnik, J., Thorne, R. M., Nishimura, Y., Angelopoulos, V., & Chen, L. (2011a). Modulation of whistler mode chorus waves: 2. Role of density variations. *Journal of Geophysical Research*, 116(A6), A06206. https://doi.org/10.1029/2010JA016313
- Li, W., & Hudson, M. K. (2019). Earth's Van Allen radiation belts: From discovery to the Van Allen probes era. Journal of Geophysical Research: Space Physics, 124(11), 8319–8351. https://doi.org/10.1029/2018JA025940
- Li, W., Ni, B., Thorne, R. M., Bortnik, J., Green, J. C., Kletzing, C. A., et al. (2013). Constructing the global distribution of chorus wave intensity using measurements of electrons by the POES satellites and waves by the Van Allen probes. *Geophysical Research Letters*, 40(17), 4526–4532. https://doi.org/10.1002/grl.50920
- Li, W., Thorne, R. M., Bortnik, J., Nishimura, Y., & Angelopoulos, V. (2011c). Modulation of whistler mode chorus waves: 1. Role of compressional pc4-5 pulsations. *Journal of Geophysical Research*, 116(A6), A06205. https://doi.org/10.1029/2010JA016312
- Li, W., Thorne, R. M., Bortnik, J., Shprits, Y. Y., Nishimura, Y., Angelopoulos, V., et al. (2011b). Typical properties of rising and falling tone chorus waves. Geophysical Research Letters, 38(14), 14103. https://doi.org/10.1029/2011GL047925
- Liu, J., Angelopoulos, V., Zhang, X. J., Runov, A., Artemyev, A., Plaschke, F., et al. (2017). Ultralow frequency waves deep inside the inner magnetosphere driven by dipolarizing flux bundles. *Journal of Geophysical Research: Space Physics*, 122(10), 10112–10128. https://doi.org/10.1002/2017JA024270
- Ma, Q., Connor, H. K., Zhang, X. J., Li, W., Shen, X. C., Gillespie, D., et al. (2020). Global Survey of plasma sheet electron precipitation due to whistler mode chorus waves in Earth's magnetosphere. Geophysical Research Letters, 47(15), e88798. https://doi.org/10.1029/2020GL088798
- Ma, Q., Li, W., Bortnik, J., Thorne, R. M., Chu, X., Ozeke, L. G., et al. (2018). Quantitative evaluation of radial diffusion and local acceleration processes during GEM challenge events. *Journal of Geophysical Research: Space Physics*, 123(3), 1938–1952. https://doi.org/10.1002/2017JA025114
- McEwen, D. J., Yee, E., Whalen, B. A., & Yau, A. W. (1981). Electron energy measurements in pulsating auroras. *Canadian Journal of Physics*, 59(8), 1106–1115. https://doi.org/10.1139/p81-146
- Meredith, N. P., Horne, R. B., & Anderson, R. R. (2001). Substorm dependence of chorus amplitudes: Implications for the acceleration of electrons to relativistic energies. *Journal of Geophysical Research*, 106(A7), 13165–13178. https://doi.org/10.1029/2000JA900156
- Meredith, N. P., Horne, R. B., Sicard-Piet, A., Boscher, D., Yearby, K. H., Li, W., & Thorne, R. M. (2012). Global model of lower band and upper band chorus from multiple satellite observations. *Journal of Geophysical Research*, 117(A10), 10225. https://doi.org/10.1029/2012JA017978
- Meredith, N. P., Horne, R. B., Thorne, R. M., & Anderson, R. R. (2003). Favored regions for chorus-driven electron acceleration to relativistic energies in the Earth's outer radiation belt. *Geophysical Research Letters*, 30(16), 160000–160001, https://doi.org/10.1029/2003GL017698
- Millan, R. M., & Thorne, R. M. (2007). Review of radiation belt relativistic electron losses. *Journal of Atmospheric and Solar-Terrestrial Physics*, 69(3), 362–377. https://doi.org/10.1016/j.jastp.2006.06.019
- Miyoshi, Y., Hosokawa, S., Kurita, S.-I., Oyama, Y., Ogawa, S., Saito, I., et al. (2021). Penetration of MeV electrons into the mesosphere accompanying pulsating aurorae. *Scientific Reports*, 11(1), 13724. https://doi.org/10.1038/s41598-021-92611-3
- Miyoshi, Y., Saito, S., Kurita, S., Asamura, K., Hosokawa, K., Sakanoi, T., et al. (2020). Relativistic electron microbursts as high-energy tail of pulsating aurora electrons. Geophysical Research Letters, 47(21), e90360. https://doi.org/10.1029/2020GL090360
- Motoba, T., Takahashi, K., Gjerloev, J., Ohtani, S., & Milling, D. K. (2013). The role of compressional Pc5 pulsations in modulating precipitation of apprentic electrons. Journal of Geophysical Pageageth: Space Physics, 118(12), 7728, 7739. https://doi.org/10.1002/201316018912
- of energetic electrons. *Journal of Geophysical Research: Space Physics*, 118(12), 7728–7739. https://doi.org/10.1002/2013JA018912

  Mourenas, D., Artemyev, A. V., Agapitov, O. V., & Krasnoselskikh, V. (2014). Consequences of geomagnetic activity on energization and loss of
- radiation belt electrons by oblique chorus waves. *Journal of Geophysical Research*, 119(4), 2775–2796. https://doi.org/10.1002/2013JA019674

  Mourenas, D., Artemyev, A. V., Zhang, X. J., Angelopoulos, V., Tsai, E., & Wilkins, C. (2021). Electron lifetimes and diffusion rates inferred from ELFIN measurements at low altitude: First results. *Journal of Geophysical Research: Space Physics*, 126(11), e29757. https://doi.org/10.1029/2021JA029757
- Mourenas, D., Zhang, X. J., Nunn, D., Artemyev, A. V., Angelopoulos, V., Tsai, E., & Wilkins, C. (2022). Short chorus wave packets: Generation within chorus elements, statistics, and consequences on energetic electron precipitation. *Journal of Geophysical Research: Space Physics*, 127(5), e30310. https://doi.org/10.1029/2022JA030310
- Mozer, F. S., Agapitov, O. V., Blake, J. B., & Vasko, I. Y. (2018). Simultaneous observations of lower band chorus emissions at the equator and microburst precipitating electrons in the ionosphere. Geophysical Research Letters, 45(2), 511–516. https://doi.org/10.1002/2017GL076120

SHI ET AL. 11 of 12

- Ni, B., Thorne, R. M., Zhang, X., Bortnik, J., Pu, Z., Xie, L., et al. (2016). Origins of the Earth's diffuse auroral precipitation. Space Science Reviews, 200(1-4), 205–259. https://doi.org/10.1007/s11214-016-0234-7
- Nishimura, Y., Bortnik, J., Li, W., Thorne, R. M., Lyons, L. R., Angelopoulos, V., et al. (2010). Identifying the driver of pulsating aurora. *Science*, 330(6000), 81–84. https://doi.org/10.1126/science.1193186
- O'Brien, T. P., Looper, M. D., & Blake, J. B. (2004). Quantification of relativistic electron microburst losses during the GEM storms. *Geophysical Research Letters*, 31(4), L04802. https://doi.org/10.1029/2003GL018621
- Orlova, K., Shprits, Y., & Spasojevic, M. (2016). New global loss model of energetic and relativistic electrons based on Van Allen probes measurements. *Journal of Geophysical Research*, 121(2), 1308–1314. https://doi.org/10.1002/2015JA021878
- Pilipenko, V., Belakhovsky, V., Kozlovsky, A., Fedorov, E., & Kauristie, K. (2014a). ULF wave modulation of the ionospheric parameters: Radar and magnetometer observations. *Journal of Atmospheric and Solar-Terrestrial Physics*, 108, 68–76. https://doi.org/10.1016/j.jastp.2013.12.015
- Pilipenko, V., Belakhovsky, V., Murr, D., Fedorov, E., & Engebretson, M. (2014b). Modulation of total electron content by ULF Pc5 waves. Journal of Geophysical Research: Space Physics, 119(6), 4358–4369. https://doi.org/10.1002/2013JA019594
- Rae, I. J., Murphy, K. R., Watt, C. E. J., Halford, A. J., Mann, I. R., Ozeke, L. G., et al. (2018). The role of localized compressional ultralow frequency waves in energetic electron precipitation. *Journal of Geophysical Research: Space Physics*, 123(3), 1900–1914. https://doi. org/10.1002/2017JA024674
- Runov, A., Sergeev, V. A., Angelopoulos, V., Glassmeier, K.-H., & Singer, H. J. (2014). Diamagnetic oscillations ahead of stopped dipolarization fronts. *Journal of Geophysical Research*, 119(3), 1643–1657. https://doi.org/10.1002/2013JA019384
- Russell, C. T., Chi, P. J., Dearborn, D. J., Ge, Y. S., Kuo-Tiong, B., Means, J. D., et al. (2008). THEMIS ground-based magnetometers. Space Science Reviews, 141(1–4), 389–412. https://doi.org/10.1007/s11214-008-9337-0
- Sandhu, J. K., Rae, I. J., Staples, F. A., Hartley, D. P., Walach, M. T., Elsden, T., & Murphy, K. R. (2021). The roles of the magnetopause and plasmapause in storm-time ULF wave power enhancements. *Journal of Geophysical Research: Space Physics*, 126(7), e29337. https://doi.org/10.1029/2021JA029337
- Shumko, M., Gallardo-Lacourt, B., Halford, A. J., Liang, J., Blum, L. W., Donovan, E., et al. (2021). A Strong correlation between relativistic electron microbursts and patchy aurora. *Geophysical Research Letters*, 48(18), e94696. https://doi.org/10.1029/2021GL094696
- Shumko, M., Sample, J., Johnson, A., Blake, B., Crew, A., Spence, H., et al. (2018). Microburst scale size derived from multiple bounces of a microburst simultaneously observed with the FIREBIRD-II CubeSats. *Geophysical Research Letters*, 45(17), 8811–8818. https://doi.org/10.1029/2018GL078925
- Streltsov, A. V., & Bengtson, M. T. (2020). Observations and modeling of whistler mode waves in the magnetospheric density ducts. *Journal of Geophysical Research: Space Physics*, 125(10), e28398. https://doi.org/10.1029/2020JA028398
- Summers, D., Ni, B., & Meredith, N. P. (2007). Timescales for radiation belt electron acceleration and loss due to resonant wave-particle interactions: 1. Theory Journal of Geophysical Research. 112(A4), 4206. https://doi.org/10.1029/2006JA011801
- Tao, X., Thorne, R. M., Li, W., Ni, B., Meredith, N. P., & Horne, R. B. (2011). Evolution of electron pitch angle distributions following injection from the plasma sheet. *Journal of Geophysical Research*, 116(A4), A04229. https://doi.org/10.1029/2010JA016245
- Thorne, R. M., Bortnik, J., Li, W., & Ma, Q. (2021). Wave–particle interactions in the Earth's magnetosphere. In *Magnetospheres in the solar system* (pp. 93–108). American Geophysical Union (AGU). https://doi.org/10.1002/9781119815624.ch6
- Thorne, R. M., Ni, B., Tao, X., Horne, R. B., & Meredith, N. P. (2010). Scattering by chorus waves as the dominant cause of diffuse auroral precipitation. *Nature*, 467(7318), 943–946. https://doi.org/10.1038/nature09467
- Tsai, E., Artemyev, A., Zhang, X.-J., & Angelopoulos, V. (2022). Relativistic electron precipitation driven by nonlinear resonance with whistler-mode waves. *Journal of Geophysical Research: Space Physics*, 127(5), e30338. https://doi.org/10.1029/2022JA030338
- Tsyganenko, N. A. (1989). A magnetospheric magnetic field model with a warped tail current sheet. *Planetary and Space Science*, 37(1), 5–20. https://doi.org/10.1016/0032-0633(89)90066-4
- Turner, D. L., Cohen, I. J., Michael, A., Sorathia, K., Merkin, S., Mauk, B. H., et al. (2021). Can Earth's magnetotail plasma sheet produce a source of relativistic electrons for the radiation belts? Geophysical Research Letters, 48(21), e95495. https://doi.org/10.1029/2021GL095495
- Wang, B., Nishimura, Y., Hartinger, M., Sivadas, N., Lyons, L. L., Varney, R. H., & Angelopoulos, V. (2020). Ionospheric modulation by storm time Pc5 ULF pulsations and the structure detected by PFISR-THEMIS conjunction. *Geophysical Research Letters*, 47(16), e89060. https://doi.org/10.1029/2020GL089060
- Watt, C. E. J., Degeling, A. W., Rankin, R., Murphy, K. R., Rae, I. J., & Singer, H. J. (2011). Ultralow-frequency modulation of whistler-mode wave growth. *Journal of Geophysical Research*, 116(A10), A10209. https://doi.org/10.1029/2011JA016730
- Wright, A. N., & Elsden, T. (2020). Simulations of mhd wave propagation and coupling in a 3-d magnetosphere. *Journal of Geophysical Research:* Space Physics, 125(2), e2019JA027589. https://doi.org/10.1029/2019JA027589
- Xia, Z., Chen, L., Dai, L., Claudepierre, S. G., Chan, A. A., Soto-Chavez, A. R., & Reeves, G. D. (2016). Modulation of chorus intensity by ULF waves deep in the inner magnetosphere. *Geophysical Research Letters*, 43(18), 9444–9452. https://doi.org/10.1002/2016GL070280
- Xia, Z., Chen, L., & Li, W. (2020). Statistical study of chorus modulations by background magnetic field and plasma density. *Geophysical Research Letters*, 47(22), e89344. https://doi.org/10.1029/2020GL089344
- Zhang, X. J., Angelopoulos, V., Artemyev, A. V., Hartinger, M. D., & Bortnik, J. (2020). Modulation of whistler waves by ultra-low-frequency perturbations: The importance of magnetopause location. *Journal of Geophysical Research: Space Physics*, 125(10), e28334. https://doi.org/10.1029/2020JA028334
- Zhang, X.-J., Angelopoulos, V., Mourenas, D., Artemyev, A., Tsai, E., & Wilkins, C. (2022a). Characteristics of electron microburst precipitation based on high-resolution elfin measurements. *Journal of Geophysical Research: Space Physics*, 127(5), e2022JA030509. https://doi.org/10.1029/2022JA030509
- Zhang, X.-J., Artemyev, A., Angelopoulos, V., Tsai, E., Wilkins, C., Kasahara, S., et al. (2022b). Superfast precipitation of energetic electrons in the radiation belts of the Earth. *Nature Communications*, 13(1), 1611. https://doi.org/10.1038/s41467-022-29291-8
- Zhang, X.-J., Chen, L., Artemyev, A. V., Angelopoulos, V., & Liu, X. (2019). Periodic excitation of chorus and ECH waves modulated by ultra-low frequency compressions. *Journal of Geophysical Research: Space Physics*, 124(11), 8535–8550. https://doi.org/10.1029/2019JA027201

SHI ET AL. 12 of 12